Tape casting of thin electrolyte and thick cathode for halide-based all-solid-state batteries

Fengyu Shen[a]*, Michael McGahan[b], John D. Pietras[b], Grace Y. Lau[a], Marca M. Doeff[a], Vincent S. Battaglia[a], Michael C. Tucker[a]*

[a]Energy Storage and Distributed Resources Division, Lawrence Berkeley National Laboratory, Berkeley, CA 94720, United States

[b]SGR North America, Saint-Gobain, Northborough, MA 01532

*Corresponding author: fshen@lbl.gov (F. Shen), mctucker@lbl.gov (M.C. Tucker)

Abstract

Most previous studies about halide solid-state electrolytes have used pellets prepared by uniaxial pressing, which is a good approach for materials development but is not suitable for commercialization. Thinner electrolyte layers that can be scaled up to large cell areas are required, and tape casting is a promising approach. It is challenging, however, as halide materials are reactive with most of the conventional solvents used in the process. In this study, solvents with low polarity, such as toluene, are found to be compatible with the Li_3YBr_6 halide material. A wide variety of candidate binders that are soluble in toluene are studied. MSB1-13 binder is preferred, based on the ionic conductivity and mechanical properties of the tape. Electrolyte tapes (<70 µm) are successfully cast on Al substrates, using 2 wt% binder. The resulting room temperature ionic conductivity is $2x10^{-4}$ S cm^{-1}. Two composite cathodes including active material ($LiFePO_4$ or $LiNi_{0.82}Mn_{0.07}Co_{0.11}O_2$) and 1 to 1.5 wt% MSB1-13 are tape cast as proof-of-concept for a scalable cell fabrication approach. A $LiFePO_4$ cell shows good retention at 25 °C. The

performance of NMC cells with tape electrolyte or pellet electrolyte is similar. This study demonstrates the feasibility of tape casting halide-based electrolytes and cathodes.

Keywords: Solid-state battery; halide; Li/In alloy; cathode; full cell;

Introduction

Binary halide solid-state electrolytes (SSEs) were discovered in the 1930s but researchers lost interest in the next several decades due to their low ionic conductivities(1). Asano et al. visited the ternary halide SSEs Li_3YCl_6 (LYC) and Li_3YBr_6 (LYB) in 2018, demonstrating high room temperature ionic conductivity (> 1 mS cm^{-1}), high voltage stability, excellent deformability, and desirable dry air stability(2). In addition to chlorides and bromides, fluorides(3), iodides(4) and even dual halogen anions-based halides(5, 6) have been synthesized by wet-chemistry(7) or solid-state synthesis methods(8). Halide SSEs have attracted attention over the past few years, as they are thought to combine the advantages of sulfide and oxide solid electrolytes(9, 10). They densify at room temperature like sulfides, but have better compatibility with high voltage cathodes, like oxide SSEs(11, 12). Halides are sensitive to moisture and decompose when exposed to humid air, but they do not evolve toxic H_2S gas, which is an issue for sulfide solid electrolytes(13). A recent report by Nazar et al. demonstrated long-term cycling of $Li_2In_{1/3}Sc_{1/3}Cl_4$ cells with a $LiNi_{0.85}Co_{0.1}Mn_{0.05}O_2$ high voltage cathode(14). The all-solid-state battery (ASSB) exhibited a long life of >3000 cycles with 80% capacity retention at room temperature. A new composition, $Li_{0.388}Ta_{0.238}La_{0.475}Cl_3$, was synthesized very recently(15). A symmetric cell containing this electrolyte and a gradient interfacial passivation layer to stabilize the lithium metal electrodes demonstrated long-term (5000 h) cycling.

The thickness of solid electrolyte films influences the energy density of ASSBs(16) as it is essentially dead weight, so should be minimized. So far most studies on halide electrolytes involve pellet-type electrolytes which are usually thicker than 300 μm(17, 18). Densification of halide pellet electrolytes usually requires high pressure (>100 MPa)(14, 19), which is impractical for large cells. It is therefore desirable to produce a thin electrolyte layer via a scalable processing technique, such as tape casting. Tape casting is a mature process for producing thin sheets in battery industries. It has been successfully used to prepare oxide thin sheet electrolytes(20, 21) and sulfide electrolytes(22), allowing higher practical energy densities to be achieved for ASSBs(23) based on them. As far as we know, fabrication of thin solid electrolyte films based on halide materials has not been reported until now. There are a few reports about tape casting halide electrolyte-containing cathodes with 1-5% binders, showing good performance(24-26).

Here, we aimed to develop a tape casting process for halide electrolytes, using LYB as a representative halide composition. This is challenging, as most conventional tape casting solvents and binders react with the halide powder. Many candidate solvents and binders were screened according to their compatibility with LYB halide, and toluene and MSB1-13 binder were selected. Thin LYB electrolytes with 2 wt% MSB1-13 were tape cast on Al substrates with thicknesses less than 70 μm. Further increasing binder content leads to free-standing and more robust electrolytes, but reduces ionic conductivity. The 2% MSB1-13 tape can be released from the substrate by punching a small area, or by laminating with a cathode layer to form a large area bilayer half-cell. A thin $LiFePO_4$ (LFP) cathode layer with a thickness of 30 to 40 μm was tape cast on an Al substrate with 1.5% MSB1-13. A thick $LiNi_{0.82}Mn_{0.07}Co_{0.11}O_2$ (NMC) cathode layer with a thickness of ~100 μm was tape cast with only 1 wt% MSB1-13. Full cells with either LFP or NMC

tape cathodes and electrolytes were assembled with Li/In alloy anodes for proof-of-concept. The LFP cell shows better capacity retention due to the lower cycling voltage window. These results demonstrate a path to commercial-scale halide ASSB fabrication.

Experimental

Powder fabrication and qualification

LYB powder was synthesized by Saint Gobain through a process involving an ammonium-containing complex metal halide. Further details on the synthesis process can be found in US Patent 11,522,217B2(27). The ionic conductivity (Figure S1) and XRD pattern (Figure 1) matches previous literature reports. Details are provided in the Supplementary Information.

Solvent and binder screening

LYB powder was mixed with various solvents with a weight ratio of 1:5, including acetonitrile (ACN), 1-butanol, cyclohexane (CH), cyclohexanone, Dimethylformamide (DMF), Dimethylsulfoxide (DMSO), heptane, hexane, methyl ethyl ketone (MEK), N-Methyl-2-pyrrolidone (NMP), toluene, and o-xylene. All the solvents were anhydrous or HPLC grade. The mixtures were stored in an Ar-filled glove box (VAC Atmospheres, <0.5 ppm H_2O and <0.5 ppm O_2, used for all studies reported here) overnight, followed by drying on a hot plate held at 120 °C in the glovebox.

LYB powder and various binders (1 to 10 wt%) were roller milled with toluene overnight. The solid loading was 35 to 50 wt%. The slurries were tape cast on Mylar or Al substrate in an Ar-filled glove box. The gap between the frame and the blade was set to 200 µm. Tapes were dried on the coater bed at 90 °C overnight.

Tape cast LYB electrolyte, LFP cathode and NMC cathode

The LYB electrolyte was tape cast by ball milling 98 wt% LYB powder and 2 wt% MSB1-13, a proprietary branched hydrocarbon polymer from Polymer Innovations, Inc.

LFP (MSE Supplies, USA), LYB, and multi walled carbon nanotubes (MWCN, MSE Supplies, USA) were mixed (50:49:1 in ratio) and additional 1.5% MSB1-13 was added. Toluene was used as the solvent and the total solid loading was 33 wt%. NMC (MSE Supplies, USA), LYB, and MWCN were mixed (60:39:1 ratio) and an additional 1% MSB1-13 was added. Toluene was used as the solvent and the solid loading was 45 wt%. The mixtures were ball milled for 2 h and tape cast on an Al substrate in an Ar-filled glove box. The doctor blade was set to 120 µm (LFP) or 200 µm (NMC). The tapes were dried on the coater bed at 90 °C overnight. We found that the LYB tape casts well but is harder to peel off when using a Mylar substrate.

Cell assembly

The Li/In alloy was prepared *ex-situ*, which is different from most literature reports where the alloy is formed during cycling from Li and In foils assembled into the cell(28, 29). Here, two layers of In metal were sandwiched around one layer of Li metal and hot pressed in a glovebox at 150 °C and 40 MPa for 10 min. The thickness of each metal layer was the same, and the total thickness after hot pressing was ~100 µm. The calculated mole ratio of Li:In is 38:62. The prepared Li/In alloy was rigid and less flexible than In or Li metal alone. According to the binary In-Li phase diagram(30), the anode was composed of InLi and extra In. Its potential vs. Li/Li^+ was ~0.62 V(28). Disks were cut from the prepared alloy for cell assembly.

For ionic conductivity measurements, LYB powder or tape was loaded in a Sphere Energy ASC-A cell (France)(31). The cell consists of PTFE ferrules for gas tightness under compression, an internal insulation sleeve to contain the tested materials, and screws on top and bottom to apply and maintain cell pressure. The cross-section area of the internal insulation is 0.5 cm^2. The applied pressure can be changed by adjusting the screws with a torque screwdriver. For symmetric cells, LYB electrolyte was first pressed at 150 MPa in an ASC-A cell and then Li/In electrodes were loaded on both sides. A stack pressure of 30 MPa was applied for testing. For full cells, cathode and electrolyte were firstly loaded and laminated with a pressure of 150 MPa. Li/In anode was lastly loaded and the stack pressure was maintained at 30 or 50 MPa. A full cell with a pellet electrolyte was assembled by loading 0.1 g LYB powder into the setup and pressed at 150 MPa. Then a tape cathode was loaded on one side and laminated at 150 MPa. Finally, the Li/In anode was loaded on the other side with a stack pressure of 50 MPa. In general, the pressure for loading Li/In alloy was lower than other assembly steps to avoid puncturing the electrolyte or causing alloy creep.

Electrochemical measurements

Electrochemical impedance spectroscopy (EIS) was conducted using a VSP300 (BioLogic, France) potentiostat with a voltage amplitude of 10 mV in the frequency range from 7 MHz to 0.1 Hz. The stainless steel plungers of an ASC-A cell acted as Li^+ blocking electrodes for the ionic conductivity measurements. Full cells were cycled between 1.88 V and 3.38 V vs. Li/In (2.5 to 4 V vs. Li/Li^+) for the LFP cathode and between 2.38 V and 3.58 V vs. Li/In (3 to 4.2 V vs. Li/Li^+) for the NMC cathode. For CV scans, Al/LYB/Li-In cells were scanned between 2 and 5 V vs. Li/In (2.62 to 5.62 V vs. Li/Li^+)

with a rate of 0.5 mV s^{-1}. All the cell tests were carried out in a thermal chamber (Model 107, TestEquity, USA) to control the temperature at 25 °C. The temperature control tolerance was ±0.5 °C.

Characterization

The cross-section and surface of samples were observed using a scanning electron microscope (SEM, JSM-7500F, JEOL, USA). Crystal structures were characterized by X-ray diffraction (XRD, D2 Phaser, Bruker, Germany), with 10° min^{-1} scanning speed at 0.02° step size. Thermogravimetric analysis in Ar atmosphere (TGA, TGA 4000, PerkinElmer, USA) was used to determine the burnout temperature of binders from room temperature to 900 °C with a heating/cooling rate of 5 °C/min.

Results and discussion

Substrate and solvent selection

The ionic conductivity of the LYB pellet is pressure-dependent and reaches a maximum of 1.4 mS cm^{-1} at room temperature after densification at high pressure (see supporting information). This is in the range of previously reported values of 0.3 to 4 mS cm^{-1} in the literature, which varies depending on synthesis method(2, 32, 33).

During tape casting and other downstream operations, as well as cell operation, the halide will contact a variety of metals. LYB was found to be compatible with the common metals aluminum, copper and stainless steel by monitoring the area specific resistance (ASR) of an LYB pellet compressed between electrodes of each metal type, Figure S2. Aluminum was chosen as the casting blade and casting substrate for this work.

As halide is incompatible with most commonly used solvents in the battery industry, such as N-Methyl-2-pyrrolidone (NMP), searching for an appropriate solvent for halide electrolyte tape casting is essential. More than 10 solvents were screened by mixing them with LYB separately overnight, then drying at 120 °C on a hot plate in a glove box. Changes to the solvent or LYB were then observed. LYB reacted with ACN, 1-butanol, cyclohexanone, DMF, DMSO, MEK and NMP exhibiting color changes or phase conversion (Figure S3 and Table S1). No changes were observed for cyclohexane, heptane, hexane, toluene and o-xylene. XRD verifies the severe reaction between LYB and DMSO, as an example, but no impurity peaks were detected from the LYB powders mixed with cyclohexane, heptane, hexane, toluene and o-xylene (Figure 1(a)). The XRD patterns were consistent with the monoclinic crystal structure previously reported(2). The compatibility between LYB powder and solvents is correlated with solvent polarity. The compatible solvents cyclohexane, heptane, hexane, toluene and xylene all have relative polarities <0.1, whereas the relative polarity of the incompatible solvents ranges from 0.281 for cyclohexanone to 0.506 for 2-butanol, Table S2. This could be ascribed to the vulnerability of halide materials to nucleophilic attack by the polar functional groups, which leads to strong interactions. In contrast, the interaction between halide materials and nonpolar or low polarity solvents are negligible(34). The ionic conductivity of the LYB powder after drying off the compatible solvents is very close to that of fresh LYB powder (Figure 1(b)), further demonstrating the compatibility. In contrast, LYB powder processed with DMSO has no measurable ionic conductivity. In summary, LYB is compatible with the low polarity solvents screened here, and toluene was selected for further development of a tape casting solvent/binder system because of its highest solubility for binders.

Binder screening

Tape casting of ceramics and metals is typically followed by binder burnout and sintering to densify the tape(20). We expect that tape casting binders that remain in the electrolyte layer will reduce the total ionic conductivity. Therefore, it is desirable to burn out the binder after tape casting, to maintain ionic conductivity of halide tapes to be near the value for pristine powder observed in pellets. Burnout temperatures of more than 20 binders were studied with TGA and some of them are shown in Figure S4(a). Among them, QPAC binders have the lowest burnout temperature of ~300 °C in Ar. To see if LYB is compatible with this burnout temperature, LYB powder was thermally treated at 300 °C in an Ar-filled glove box for 2 h. Unfortunately, the LYB powder partially decomposed, demonstrated by peak splitting and new peaks in the XRD pattern (Figure S4(b)). The ionic conductivity of the thermally treated LYB is 7.2×10^{-5} S cm^{-1} (Figure S4(c)), which is only one twentieth of the pristine powder's conductivity. Thus, binder burnout is ruled out as a processing approach, unless new binders with lower burnout temperatures can be identified.

The binder will remain in the cast layers throughout the lifetime of the battery cell. The next step, therefore, is selection of a tape casting binder that is soluble in a low polarity solvent, and compatible with LYB during cell fabrication and operation. Binders used in the battery industry, such as polyvinylidene fluoride (PVDF), and many common tape casting binders, such as polyvinyl acetate (PVA) or polyvinyl butyral (PVB), do not dissolve in these low polarity solvents. Compared to the other compatible solvents, toluene provides the highest solubility for binders based on our experiments. Thus, it was selected as the solvent for the following halide tape casting development. More than 10 candidate binders were ball milled separately with LYB powder in

toluene. The resulting LYB slurries were tape cast on Al substrate in a glove box and subsequently dried on the coater bed. All the selected binders, QPAC100, QPAC130, ethyl cellulose, PEO, PMMA, polyethylenimine, MSB1-13, polystyrene, polybutadiene and poly(acrylonitrile-co-butadiene) show good compatibility with LYB. In the tapes, color change is not observed, and the XRD shows that the LYB structure is unchanged (Figure 1(c)). The ionic conductivity of the LYB tapes is 1 to 4 orders of magnitude lower than the fresh powder, depending on the binder type and content. Ionic conductivity decreases with increased binder content for the same binder. This impact on conductivity is expected, as the non-conductive binder partially coats the LYB powder and reduces ion transfer between adjacent particles. The tapes with PEO, polyethylenimine, MSB1-13, polystyrene or poly(acrylonitrile-co-butadiene) as the binder show good ionic conductivity (Table 1). Considering mechanical properties, such as strength, elongation, flexibility and robustness after lamination, MSB1-13 was selected as the binder for further tape casting optimization. Note that the slurries prepared here were not optimized, but used only as a screening tool. In addition to MSB1-13, some of the other binder candidates are expected to be viable with further optimization effort.

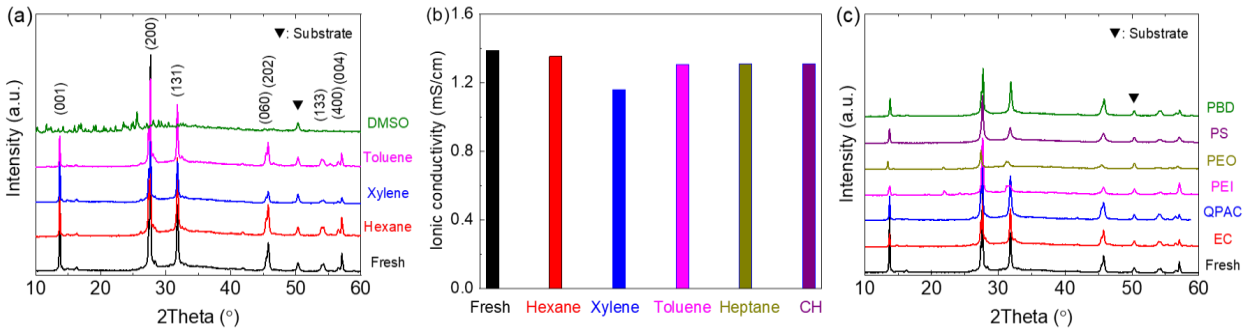

Figure 1. Compatibility of LYB with solvents and binders. (a) XRD patterns and (b) ionic conductivity of LYB fresh powder and solvent-processed powders; (c) XRD patterns of LYB tape cast with selected binders in toluene, showing good compatibility.

Table 1. Ionic conductivity of LYB tapes with binders, cast from toluene slurries.

Binder	Ionic conductivity (S cm^{-1})	Tape quality
2% QPAC100+1.7% polycarbonate	$3.4x10^{-5}$	Cracked
5% QPAC100	$3.2x10^{-6}$	Flexible
10% QPAC100	$2.5x10^{-6}$	Strong flexible
3% QPAC130	$9.7x10^{-5}$	Brittle
3% ethyl cellulose (46 cP)	$4.3x10^{-5}$	Cracked
2.5% ethyl cellulose (300 cP)	$9.1x10^{-5}$	Cracked
2.5% PEO	$1.7x10^{-4}$	Brittle
3% PEO	$1.5x10^{-4}$	Brittle
3% PMMA	$1.0x10^{-5}$	Brittle
2.5% polyethylenimine	$2.2x10^{-4}$	Cracked
1% MSB1-13	$3.5x10^{-4}$	Brittle
1.5% MSB1-13	$2.6x10^{-4}$	Brittle
2% MSB1-13	$2.0x10^{-4}$	Flexible
3% MSB1-13	$6.3x10^{-5}$	Flexible
5% MSB1-13	$1.9x10^{-5}$	Strong flexible
10% MSB1-13	$2.4x10^{-7}$	Strong flexible
2.5% polystyrene	$3.2x10^{-4}$	Brittle
3% polystyrene	$1.4x10^{-4}$	Brittle
3% polybutadiene	$6.2x10^{-6}$	Flexible
3% poly(acrylonitrile-co-butadiene)	$1.1x10^{-4}$	Flexible

The impact of MSB1-13 content on tape quality and ionic conductivity is shown in Figure 2. With increasing binder content there is a trade-off: mechanical properties improve significantly, but ionic conductivity decreases approximately logarithmically. At 1 and 1.5 wt% MSB1-13 loading, the tapes are very challenging to peel off from the Al substrate although their ionic conductivities remain high: $3.5x10^{-4}$ and $2.6x10^{-4}$ S cm^{-1}, respectively. When the binder content is increased to 2 wt%, the tape is still not free-standing in large area but it can be peeled off from the Al substrate

when it is punched into a small area (<1.6 cm^2). Large area tapes could be successfully stripped from the substrate by first laminating with a cathode tape (discussed below). When the binder content is further increased to 5 wt% or 10 wt%, large-area free-standing tapes are achieved, but with an unacceptable sacrifice of ionic conductivity. Based on these results, 2 wt% MSB1-13 was chosen for preparing tapes for integration into cells.

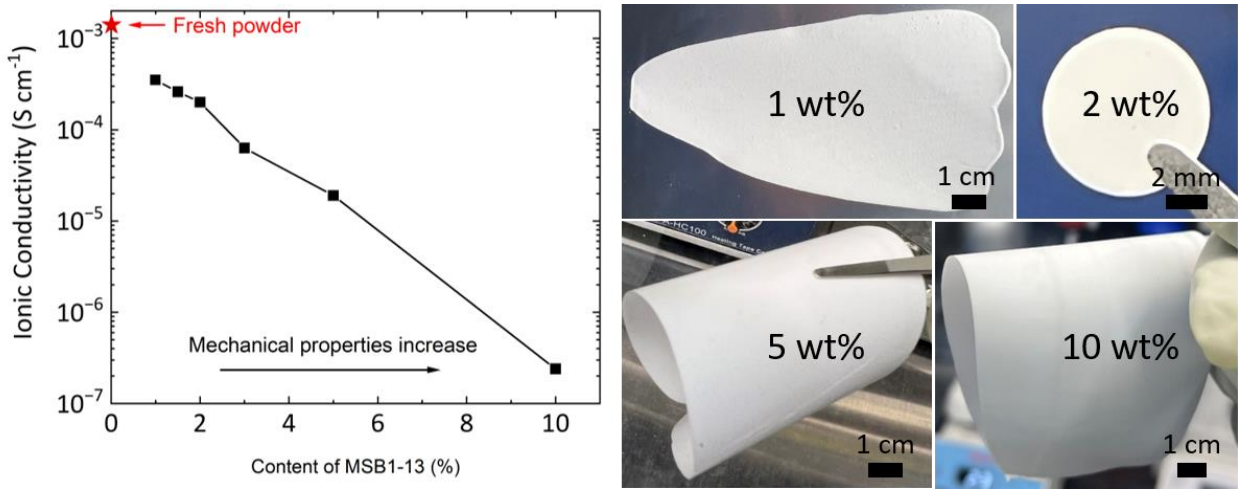

Figure 2. Impact of binder loading for MSB1-13. (left) Ionic conductivity vs. MSB1-13 content. (right) Images of tapes with various binder loadings. Note that the tape with 1 wt% binder was still able to detach from the Al substrate but very brittle.

To assess the long-term stability of the LYB-binder mixture, an LYB tape with 2 wt% MSB1-13 was stored in an Ar-filled glove box for 6 months. Electrolyte samples were punched from the tape and characterized by EIS and XRD. Figure 3(a) shows that the aged tape at 6 months has similar ionic conductivity to the fresh tape. XRD patterns shown in Figure 3(b) demonstrate no decomposition of the aged LYB tape compared to the fresh tape. The peak shift is ascribed to the specimen height difference in the sample holder. Thus, MSB1-13 binder is compatible with LYB even during long term aging.

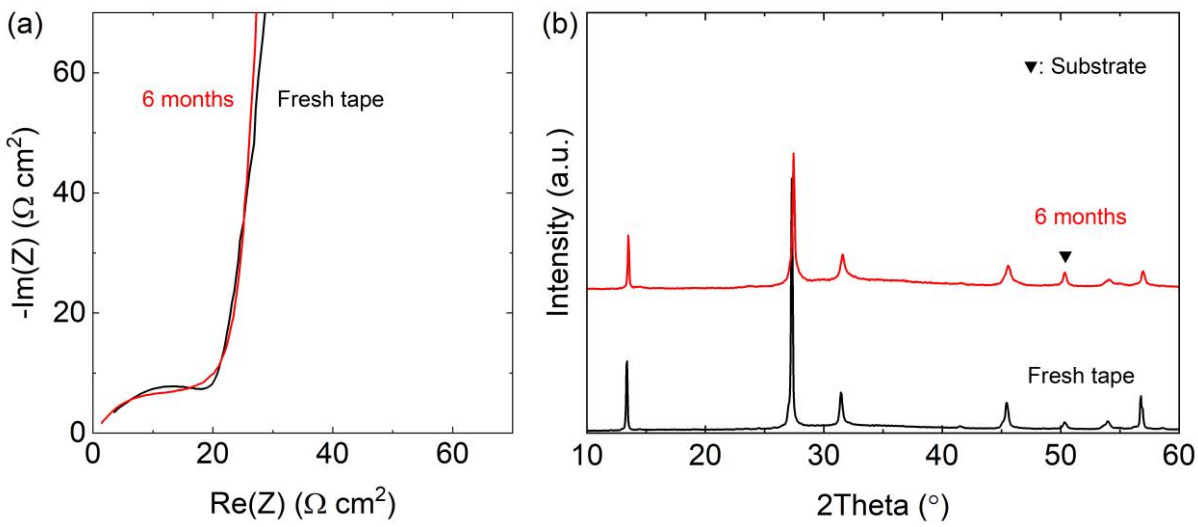

Figure 3. Aging of LYB tape. (a) EIS and (b) XRD patterns of LYB tapes with 2 wt% MSB1-13 sealed in an Ar-filled glove box. The tape thickness is 38-40 µm.

Symmetric cells

To evaluate the stability and critical current density of the LYB tape, symmetric cells were fabricated and tested with Li/In alloy electrodes. An LYB tape with 2 wt% MSB1-13 binder was tape cast on an Al substrate, with thickness of ~65 µm (Figure 4(a,b)). A circular electrolyte disk was punched with a diameter of 5/16 inch (area ~0.5 cm^2), and detached from the Al substrate. The resulting free-standing LYB electrolyte was densified at room temperature with a pressure of 150 MPa for several minutes. Punched Li/In alloy electrodes with the same area were used to avoid reduction of LYB at low potential (<~0.6 V)(35). Two symmetric cells were assembled in Sphere Energy ASC-A cells with a stack pressure of 30 MPa and the pressure was maintained during cycling. One cell was cycled by reversibly plating the Li in both directions while the current was increased stepwise at 25 °C (Figure 4(c)). Although the polarization potential increased dramatically at high currents, the cell was not shorted even after cycling at 1.5 mA cm^{-2} (1.5 mAh

cm^{-2}). These asymmetric voltage profiles usually occur under high current densities, which could be ascribed to the formation of voids at the electrode/electrolyte interfaces(36-38).

The critical current density (CCD) therefore appears to exceed 1.5 mA cm^{-2}. Note that the full cells discussed below were cycled at significantly lower current densities (<= 0.3 mA cm^{-2}). Another cell was cycled at constant current for more than 170 cycles, as shown in Figure 4(d). The potential increased in the initial several cycles at 0.1 mA cm^{-2} and stabilized after that. The potential increased from ~210 mV to ~225 mV after 100 cycles at 0.5 mA cm^{-2}. Generally, the symmetric cells with tape cast LYB electrolytes are stable and tolerate moderate current densities.

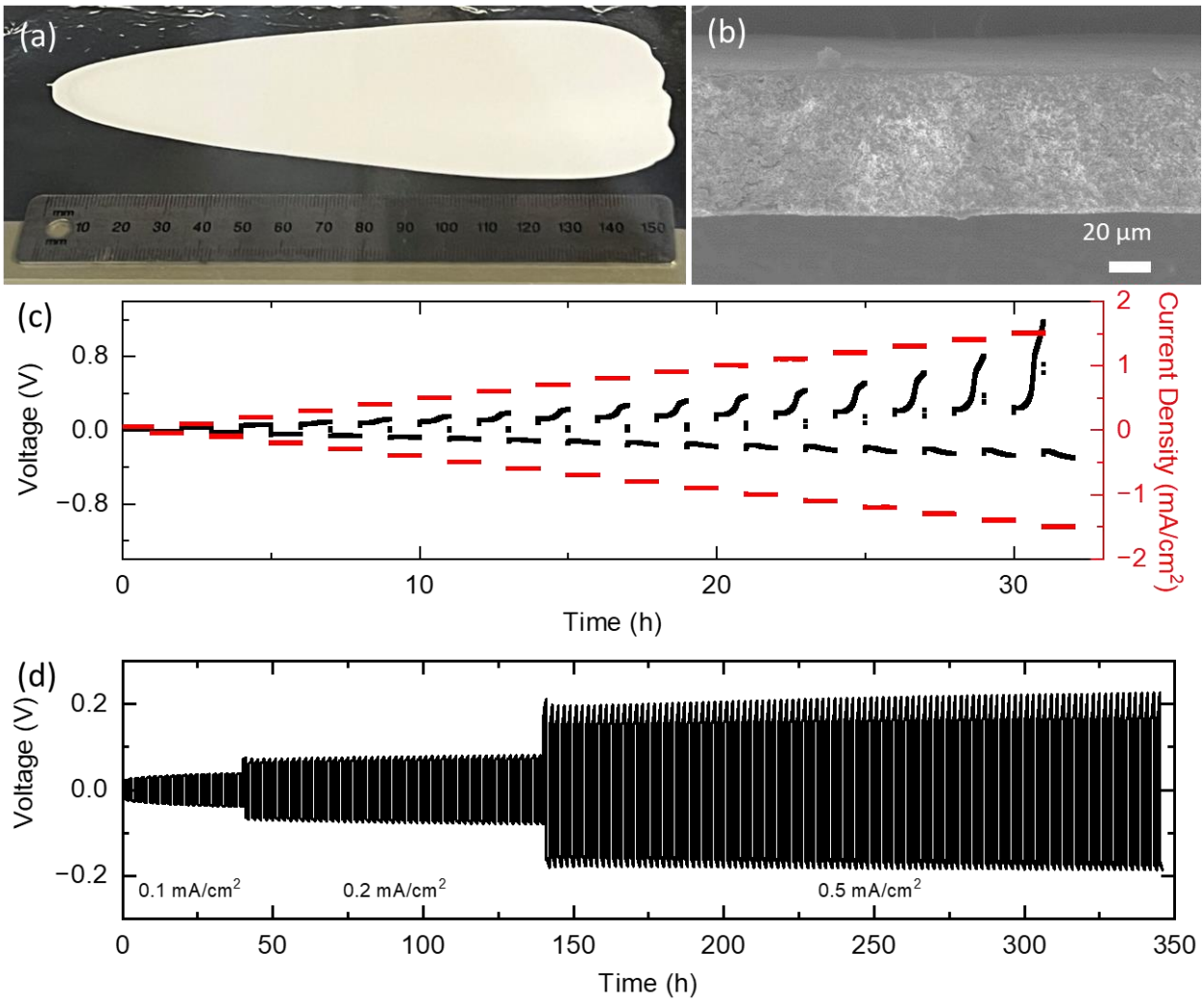

Figure 4. LYB tape with 2 wt% MSB1-13. (a) Digital picture of LYB tape on Al substrate and (b) its cross-section SEM image; (c) Voltage vs. step current density; (d) Li/In symmetric cell plated/stripped at 0.1 to 0.5 mA cm^{-2}.

Full cells

To further verify that tape casting is viable for preparing full cells, two types of cathode tapes with halide catholyte and LFP or NMC were prepared by the same tape casting process used for the LYB electrolyte. The LFP cathode is uniform and each component is well-distributed in the tape (Figure 5(a, b)). Due to the small particle size of LFP (<1 µm), it is very challenging to tape

cast a crack-free thick cathode (100 µm) with a small binder content (1.5 wt%). Here, the thickness of the cathode is only ~35 µm to avoid cracking. To increase areal capacity, two layers of LFP cathode were laminated to a LYB electrolyte at room temperature and 150 MPa for several minutes. The cathode active material (CAM) loading for this cell was 7.5 mg cm^{-2}. The multi-layer tapes show good contact (Figure 5(c)). No voids or delamination were observed from the cross-section view. A full cell with the laminated LFP cathode/LYB and Li/In anode was assembled with a stack pressure of 30 MPa. The cell was cycled in the voltage range of 1.88 to 3.38 V vs. Li/In (2.5 to 4.0 V vs. Li/Li^+) at 0.1 C (corresponding to 0.13 mA cm^{-2} assuming a theoretical capacity of 175 mAh/g), 0.2 C, 0.05 C and 0.02 C in sequence, with initial discharge capacities of 63.1, 41.4, 79.1 and 93.1 mAh g^{-1}, respectively. The cell shows good retention at 0.1 C over 20 cycles with Coulombic efficiency >98%. Despite the low capacity, this test demonstrates the cyclability of the tape cast and laminated cathode/electrolyte cell.

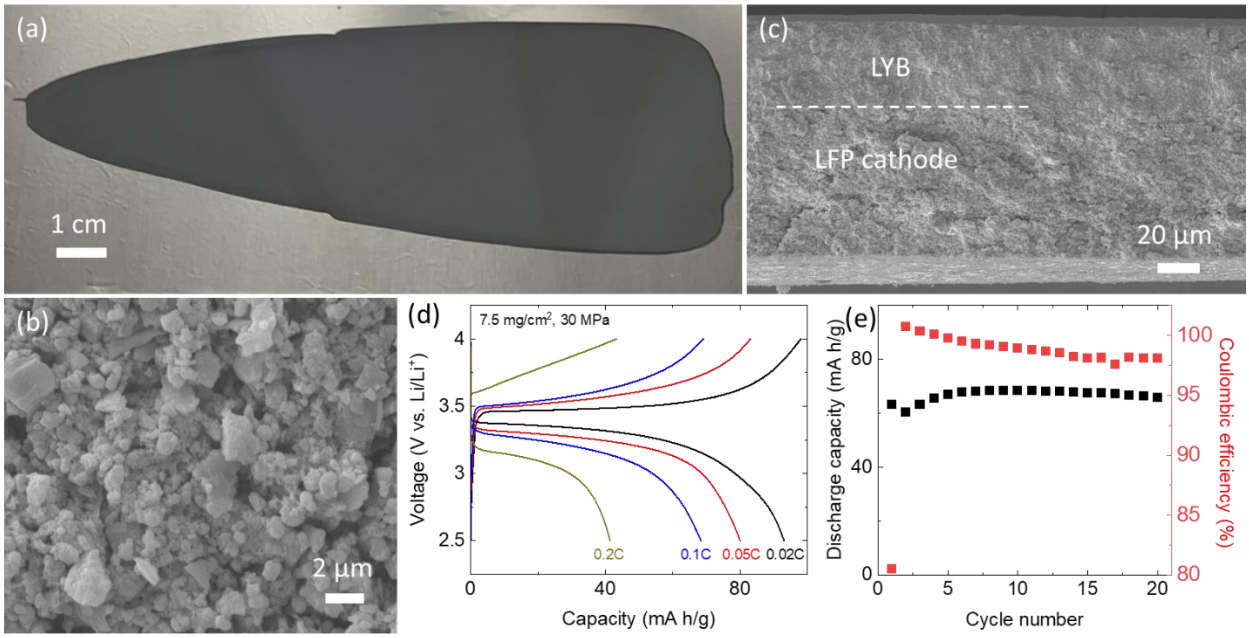

Figure 5. LFP cathode. (a) Digital image of LFP cathode tape on Al substrate; (b) SEM image of LFP cathode surface; (c) cross-section SEM image of LFP (2 layers)/LYB bi-layer structure; (d) Charge/discharge curves at 0.02, 0.05, 0.1 and 0.2 C and (d) capacity retention at 0.1 C.

Another cathode with NMC as the active material was also prepared by tape casting. A crack-free cathode with a thickness around 100 μm was achieved, even though only 1 wt% binder was added. This is due to the large particle size (3 to 5 μm) of the NMC cathode material. A single layer of NMC cathode was laminated with a LYB electrolyte layer at room temperature and 150 MPa for several minutes. The cathode layer is thicker than the electrolyte layer and both layers show good contact (Figure 6(a, b)). The CAM loading is 14 mg cm^{-2}. The cell was cycled at 0.1 C (corresponding to 0.28 mA cm^{-2} assuming a theoretical capacity of 200 mAh/g) with a stack pressure of 50 MPa. As shown in Figure 6(c), the cell fades quickly. The 1^{st} cycle capacity is 93.2 mAh g^{-1}. The discharge capacity at the 10^{th} cycle is only ~50% of the 1^{st} cycle. As a comparison, a cell with a pellet electrolyte and a tape cathode was assembled with a similar CAM loading of 15 mg cm^{-2} (corresponding to 0.3 mA cm^{-2}). The cell was cycled at the same pressure and C rate. Its capacity is very similar to the cell with the tape electrolyte. The similar behavior of the cells with pellet and tape electrolytes supports the viability of the tape electrolyte prepared by tape casting, and suggests the cell performance and durability are limited by the cathode.

The fast fading of the two NMC cells is partially ascribed to the well-known oxidative instability of the LYB electrolyte at the high cutoff potential(35). Oxidative degradation of LYB during cyclic voltammetry is apparent above ~3.9 V vs. Li/Li^+, Figure 7. Addition of the MSB1-13 binder does not narrow the voltage window (oxidation still starts at ~3.9 V vs. Li/Li^+). The stable voltage window is expanded after the first cycle, likely due to irreversible reactions forming a passivating film during the first cycle. Replacing LYB with another halide material with a wider voltage stability window is anticipated to improve capacity retention, and this materials development

will be reported in the future. These results demonstrate that tape casting is viable to prepare halide-based solid-state batteries with thin electrolytes and thick cathodes, with further optimization.

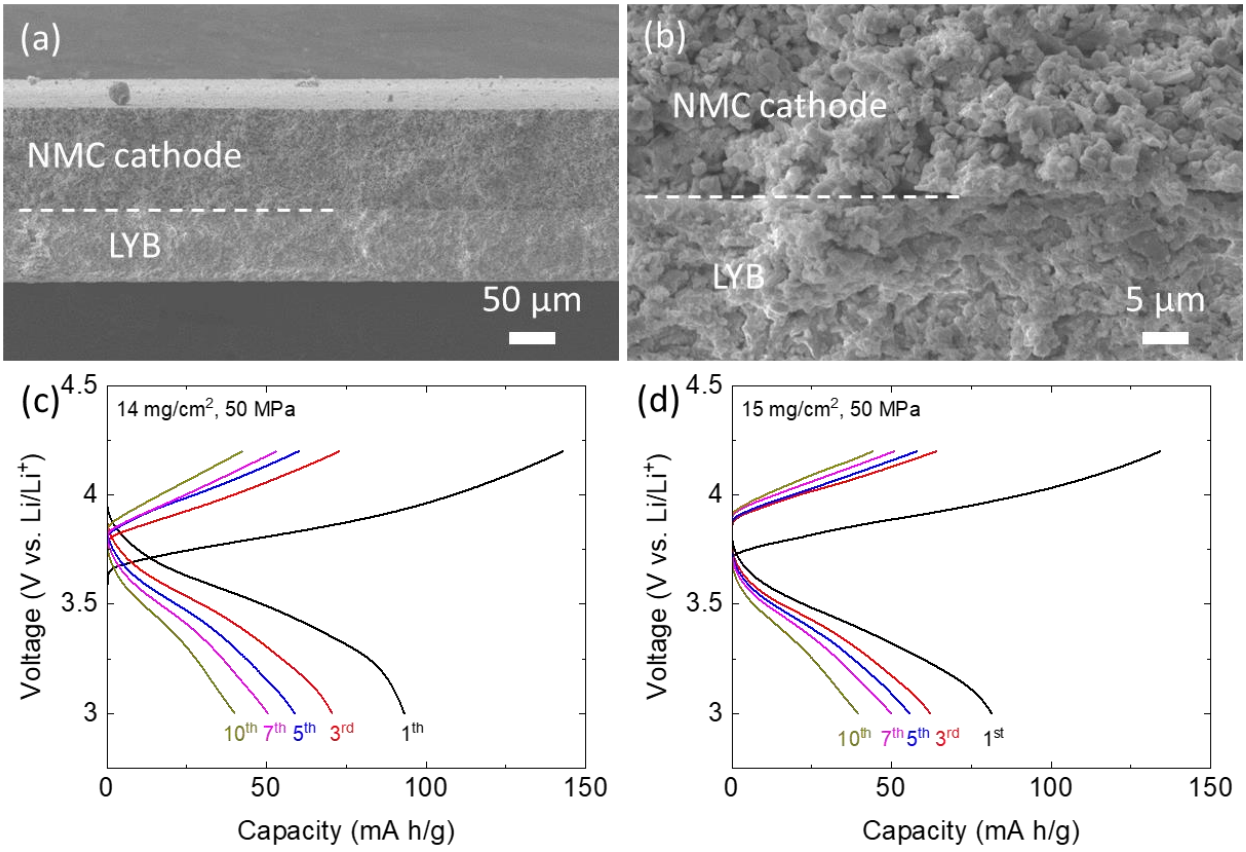

Figure 6. NMC cathode. Cross-section SEM images of NMC/LYB bi-layer structure at (a) low and (b) high magnification; Charge/discharge curves for NMC tape cathode at 0.1 C and 25 °C with (c) tape cast electrolyte and (d) pellet electrolyte.

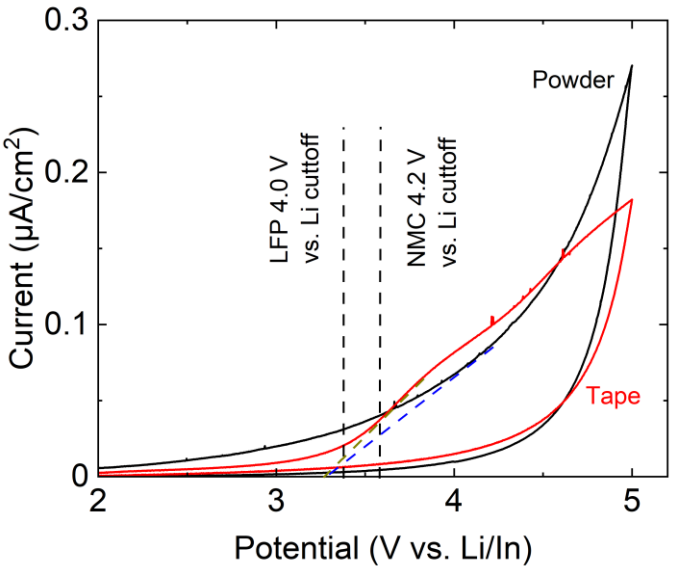

Figure 7. CV of LYB pellet (black lines) and tape (red lines) electrolytes with a scan rate of 0.5 mV s^{-1} at 25 °C. Working electrode is Al.

Conclusions

A tape casting system was developed for halide SSBs. This study demonstrates that tape casting is viable to prepare large-area thin halide electrolytes and thick composite cathodes. Halide materials are very reactive, and solvents and binders were screened for compatibility with LYB. Solvents with low polarity were found to be compatible with LYB and toluene was selected for slurry development. MSB1-13 was selected as the binder for tape casting due to long term compatibility, low impact on ionic conductivity, and good mechanical properties. The preferred binder content was found to be 2 wt%, based on the tradeoff between ionic conductivity and mechanical properties. Large area LYB tapes with thicknesses <70 µm were prepared. Cathode layers were also tape cast with the same solvent and binder. A cell containing an LFP cathode ~70 µm thick tape cast with 1.5 wt% binder showed good capacity retention. In contrast, a cell with an NMC cathode ~100 µm thick tape cast with 1 wt% binder faded rapidly, most likely due to the

oxidative instability of the electrolyte at the high cutoff potential. We expect further improvements with selection of more oxidatively stable halides and/or the use of coated cathode particles.

Acknowledgments

This work was funded by the Vehicle Technologies Office, Advanced Materials and Manufacturing Technologies Office, Office of Energy Efficiency and Renewable Energy, of the U.S. Department of Energy, under Contract Number DE-AC02-05CH11231. The views and opinions of the authors expressed herein do not necessarily state or reflect those of the United States Government or any agency thereof. Neither the United States Government nor any agency thereof, nor any of their employees, makes any warranty, expressed or implied, or assumes any legal liability or responsibility for the accuracy, completeness, or usefulness of any information, apparatus, product, or process disclosed, or represents that its use would not infringe privately owned rights.

Reference

1. D. C. Ginnings and T. E. Phipps, *J Am Chem Soc*, **52**, 1340 (1930).
2. T. Asano, A. Sakai, S. Ouchi, M. Sakaida, A. Miyazaki and S. Hasegawa, *Adv Mater*, **30** (2018).
3. J. L. Hu, K. Y. Chen and C. L. Li, *Acs Appl Mater Inter*, **10**, 34322 (2018).
4. Z. M. Xu, X. Chen, K. Liu, R. H. Chen, X. Q. Zeng and H. Zhu, *Chem Mater*, **31**, 7425 (2019).
5. E. Umeshbabu, S. Maddukuri, Y. Hu, M. Fichtner and A. R. Munnangi, *Acs Appl Mater Inter*, **14** (2022).
6. T. W. Yu, J. W. Liang, L. Luo, L. M. Wang, F. P. Zhao, G. F. Xu, X. T. Bai, R. Yang, S. Q. Zhao, J. T. Wang, J. Q. Yu and X. L. Sun, *Adv Energy Mater*, **11** (2021).
7. C. H. Wang, J. W. Liang, J. Luo, J. Liu, X. N. Li, F. P. Zhao, R. Y. Li, H. Huang, S. Q. Zhao, L. Zhang, J. T. Wang and X. L. Sun, *Sci Adv*, **7** (2021).
8. Y. Nikodimos, W. N. Su and B. J. Hwang, *Adv Energy Mater*, **13** (2023).
9. H. Kwak, S. Wang, J. Park, Y. S. Liu, K. T. Kim, Y. Choi, Y. F. Mo and Y. S. Jung, *Acs Energy Lett*, **7**, 1776 (2022).

10. X. N. Li, J. W. Liang, X. F. Yang, K. R. Adair, C. H. Wang, F. P. Zhao and X. L. Sun, *Energ Environ Sci*, **13**, 1429 (2020).
11. F. Y. Shen, R. A. Jonson and M. C. Tucker, *J Mater Chem A*, **10**, 25159 (2022).
12. F. Y. Shen, R. A. Jonson, D. Y. Parkinson and M. C. Tucker, *J Am Ceram Soc*, **105**, 90 (2022).
13. H. Muramatsu, A. Hayashi, T. Ohtomo, S. Hama and M. Tatsumisago, *Solid State Ionics*, **182**, 116 (2011).
14. L. D. Zhou, T. T. Zuo, C. Y. Kwok, S. Y. Kim, A. Assoud, Q. Zhang, J. Janek and L. F. Nazar, *Nat Energy*, **7**, 83 (2022).
15. Y.-C. Yin, J.-T. Yang, J.-D. Luo, G.-X. Lu, Z. Huang, J.-P. Wang, P. Li, F. Li, Y.-C. Wu, T. Tian, Y.-F. Meng, H.-S. Mo, Y.-H. Song, J.-N. Yang, L.-Z. Feng, T. Ma, W. Wen, K. Gong, L.-J. Wang, H.-X. Ju, Y. Xiao, Z. Li, X. Tao and H.-B. Yao, *Nature*, **616**, 77 (2023).
16. J. Y. Wu, L. X. Yuan, W. X. Zhang, Z. Li, X. L. Xie and Y. H. Huang, *Energ Environ Sci*, **14** (2021).
17. M. Balaish, J. C. Gonzalez-Rosillo, K. J. Kim, Y. T. Zhu, Z. D. Hood and J. L. M. Rupp, *Nat Energy*, **6**, 227 (2021).
18. H. Kwak, D. Han, J. Lyoo, J. Park, S. H. Jung, Y. Han, G. Kwon, H. Kim, S. T. Hong, K. W. Nam and Y. S. Jung, *Adv Energy Mater*, **11** (2021).
19. S. Kim, H. Y. Y. Cha, R. Kostecki and G. Y. Chen, *Acs Energy Lett* (2022).
20. R. A. Jonson, E. Yi, F. Y. Shen and M. C. Tucker, *Energ Fuel*, **35**, 8982 (2021).
21. M. Jabbari, R. Bulatova, A. I. Y. Tok, C. R. H. Bahl, E. Mitsoulis and J. H. Hattel, *Mater Sci Eng B-Adv*, **212**, 39 (2016).
22. B. Emley, Y. L. Liang, R. Chen, C. S. Wu, M. Pan, Z. Fan and Y. Yao, *Mater Today Phys*, **18** (2021).
23. Y. G. Lee, S. Fujiki, C. Jung, N. Suzuki, N. Yashiro, R. Omoda, D. S. Ko, T. Shiratsuchi, T. Sugimoto, S. Ryu, J. H. Ku, T. Watanabe, Y. Park, Y. Aihara, D. Im and I. T. Han, *Nat Energy*, **5**, 299 (2020).
24. K. Wang, Q. Ye, J. Zhang, H. Huang, Y. P. Gan, X. P. He and W. K. Zhang, *Front Mater*, **8** (2021).
25. X. H. Li, Q. Ye, Z. Wu, W. K. Zhang, H. Huang, Y. Xia, Y. P. Gan, X. P. He, X. H. Xia and J. Zhang, *Electrochim Acta*, **453** (2023).
26. Q. Ye, X. H. Li, W. K. Zhang, Y. Xia, X. P. He, H. Huang, Y. P. Gan, X. H. Xia and J. Zhang, *Acs Appl Mater Inter*, **15**, 18878 (2023).
27. V. Ouspenski and G. Assat, Electrolyte material and methods of forming, in, US (2021).
28. A. L. Santhosha, L. Medenbach, J. R. Buchheim and P. Adelhelm, *Batteries Supercaps*, **2**, 524 (2019).
29. L. M. Riegger, R. Schlem, J. Sann, W. G. Zeier and J. Janek, *Angew Chem Int Edit*, **60**, 6718 (2021).
30. J. Songster and A. D. Pelton, *Journal of Phase Equilibria*, **12**, 37 (1991).
31. https://sphere-energy.eu/all-solid-state-test-cell, accessed 9/6/2023.
32. C. Yu, Y. Li, K. R. Adair, W. H. Li, K. Goubitz, Y. Zhao, M. J. Willans, M. A. Thijs, C. H. Wang, F. P. Zhao, Q. Sun, S. X. Deng, J. W. Liang, X. N. Li, R. Y. Li, T. K. Sham, H. Huang, S. G. Lu, S. Q. Zhao, L. Zhang, L. van Eijck, Y. N. Huang and X. L. Sun, *Nano Energy*, **77** (2020).
33. R. Schlem, A. Banik, S. Ohno, E. Suard and W. G. Zeier, *Chem Mater*, **33**, 327 (2021).
34. Y. Nikodimos, C. J. Huang, B. W. Taklu, W. N. Su and B. J. Hwang, *Energ Environ Sci*, **15**, 991 (2022).
35. Y. Qie, S. Wang, S. J. Fu, H. H. Xie, Q. Sun and P. R. Jena, *J Phys Chem Lett*, **11**, 3376 (2020).
36. K. Lee, E. Kazyak, M. J. Wang, N. P. Dasgupta and J. Sakamoto, *Joule*, **6**, 2547 (2022).
37. J. W. Meng, Y. Zhang, X. J. Zhou, M. Lei and C. L. Li, *Nat Commun*, **11** (2020).
38. W. X. Ji, D. Zheng, X. X. Zhang, T. Y. Ding and D. Y. Qu, *J Mater Chem A*, **9**, 15012 (2021).